AGU PUBLICATIONS

Geophysical Research Letters

RESEARCH LETTER

10.1002/2014GL061787

Key Points:
- Model cyclotron resonant interactions using a finite difference Vlasov solver
- Model linear and nonlinear growth in agreement with theory and observations
- Clearly resolve phase-space hole during nonlinear growth compared to PIC method

Correspondence to:
V. Harid,
vharid@stanford.edu

Citation:
Harid, V., M. Gołkowski, T. Bell, J. D. Li, and U. S. Inan (2014), Finite difference modeling of coherent wave amplification in the Earth's radiation belts, *Geophys. Res. Lett.*, *41*, doi:10.1002/2014GL061787.

Received 1 OCT 2014
Accepted 13 OCT 2014
Accepted article online 21 OCT 2014

Finite difference modeling of coherent wave amplification in the Earth's radiation belts

V. Harid[1], M. Gołkowski[2], T. Bell[1], J. D. Li[1], and U. S. Inan[1,3]

[1]Department of Electrical Engineering, Stanford University, Stanford, California, USA, [2]Department of Electrical Engineering, University of Colorado Denver, Denver, Colorado, USA, [3]Department of Electrical Engineering, Koc University, Istanbul, Turkey

Abstract Modeling of gyroresonant wave-particle interactions in the radiation belts requires solving the Vlasov-Maxwell system of equations in an inhomogenous background geomagnetic field. Previous works have employed particle-in-cell methods or Eulerian solvers (such as the Vlasov Hybrid Simulation code) to provide numerical solutions to the problem. In this report, we provide an alternative numerical approach by utilizing a first order finite difference upwind scheme. When coupled to the narrowband Maxwell's equations, the model reproduces linear as well as nonlinear wave growth of coherent signals. Wave growth is nonlinear growth when the wave amplitude exceeds the minimum value for phase trapping of counterstreaming particles and is linear otherwise. The model also demonstrates free-running frequency variation for a case with a high linear growth rate. In addition, the model confirms the theoretical prediction of a stable "phase-space hole" during the nonlinear growth process. The plasma parameters and L shell used in this study are typical of those associated with the Siple Station wave injection experiment.

1. Introduction

Whistler mode waves in the magnetosphere play an important role in the energization as well as loss of energetic electrons in the Earth's radiation belts [*Abel and Thorne*, 1998; *Thorne*, 2010]. Accurate modeling of the problem requires tracking a distribution of energetic electrons in phase space while self-consistently capturing the electromagnetic waves that will propagate through the background cold magnetized plasma and be amplified by the hot plasma component. The evolution of the particle distribution function is governed by the Vlasov equation while the wave fields are generated according to Maxwell's equations.

Under the assumption of small amplitude waves, the Vlasov-Maxwell set of equations can be linearized and solved analytically. Linear theory predicts that whistler mode waves of a given frequency can be amplified provided that the energetic electron distribution has sufficient pitch angle anisotropy at the Doppler-shifted cyclotron resonance velocity [*Kennel and Petschek*, 1966]. Coherent whistler mode waves, in particular, can grow to large amplitudes at which point resonant electrons can be phase trapped and the interaction becomes strongly nonlinear [*Nunn*, 1974; *Omura et al.*, 1991]. The coherent wave instability is believed to be responsible for the generation of discrete VLF emissions known as magnetospheric chorus which can in turn energize electrons or precipitate them onto the neutral atmosphere [*Bortnik and Thorne*, 2007; *Thorne et al.*, 2010, 2013]. Amplification of injected VLF signals, such as in the case of the Siple Station wave injection experiment, can result in new coherent waves free running in frequency known as triggered emissions [*Helliwell*, 1983]. Quantifying wave amplification in the nonlinear regime is difficult to accomplish with analytical techniques, and accurate numerical modeling is indispensable. Analytical and numerical modeling of coherent wave-particle interactions have been addressed by several authors [*Bell and Buneman*, 1964; *Kennel and Petschek*, 1966; *Nunn*, 1974; *Hikishima et al.*, 2010; *Albert et al.*, 2012; *Harid et al.*, 2014].

Particle-in-cell (PIC) methods solve the Vlasov equation by using a large number of superparticles and are used extensively in space plasma physics. PIC simulations have been successfully used to model rising tone triggered emissions as well as discrete chorus emissions [*Katoh and Omura*, 2006, 2007; *Omura et al.*, 2008; *Hikishima et al.*, 2010, 2009]. *Katoh and Omura* [2006] used a hybrid particle code that treats the background cold plasma as a fluid while the energetic electrons are treated as particles in a PIC code. They found that triggering of a rising tone occurs at the back end of the input signal close to the magnetic equator, and the resonant current formation by untrapped electrons plays an important role in the triggering process. Using the same simulation procedure, *Omura et al.* [2008] showed that chorus elements with rising tones are

generated close to the magnetic equator and undergo further nonlinear growth while propagating away while the wave frequency stays essentially the same. *Hikishima et al.* [2010] used a full particle code with no approximations to Maxwell's equations to simulate rising tone emissions. A monochromatic signal injected at the magnetic equator was shown to trigger a rising emission. The triggering signal created a depletion of electrons at the resonant velocity while the electrons exiting the wave trap generated a new wave rising in frequency. Although PIC simulations have been extremely successful at modeling wave-particle interactions in the radiation belts, the primary concern is including enough particles to accurately sample phase space such that all the physically relevant particles are taken into account (i.e., electrons close to resonance). This often requires spending computational resources on a large number of particles that may not contribute significantly to wave growth.

Eulerian methods have also been used to model the coherent wave instability by solving the Vlasov equation directly on a grid in phase space [*Filbet and Sonnendrücker*, 2003]. The Vlasov Hybrid Simulation (VHS) code, as described in *Nunn* [1993], has been successfully used to model the dynamic spectra of VLF-triggered emissions. In this technique, single-particle trajectories are traced continuously through time while the distribution function is obtained by interpolating onto a phase-space grid at each time step. Once the distribution function is known, the resonant currents are calculated and used to determine the wave fields. The VHS code has the advantage of having a dynamic number of simulation particles and hence does not suffer from the large number of particles required in PIC methods. The VHS code has been used to model rising, falling, and hook-like emissions [*Nunn et al.*, 2003]; however, rising emissions are most commonly observed in the simulations [*Nunn et al.*, 1997]. The code has been employed in several studies over the past few decades. *Nunn and Smith* [1996] simulated whistler-triggered emissions using the VHS code and demonstrated both rising and falling tones triggered in good agreement with observations. *Nunn et al.* [2005] considered a parametric study of the VHS code over a range of simulation parameters. It was found that low input amplitudes generated fallers, intermediate amplitudes generated risers, and large amplitudes generated fallers, hooks, or oscillating tones. The frequency sweep rate was shown to be most sensitive to the cold plasma density with lower densities giving higher sweep rates. *Nunn and Omura* [2012] modified the VHS code by restricting the interaction region to be only upstream of the equator where the inhomogeneity is positive. With the modification, the VHS code produced stable falling tones with the resonant particle trap showing an enhanced distribution function (hill) in contrast to a depletion caused by a rising emission. The component of the resonant current parallel to wave magnetic field was shown to be positive for falling tones while it is negative for rising tones. Although the VHS code has been used to simulate various aspects of triggered emissions, phenomena such as saturation and multiwave interactions are difficult to reproduce with this model. Additionally, the artificial filtering required to keep the simulation stable may unintentionally swamp physical effects. *Gibby et al.* [2008] also used a Vlasov hybrid technique to simulate nonlinear growth; however, a backward semi-Lagrangian procedure was used such that the particle trajectories were restarted at each time step. The model was able to produce nonlinear growth as well as saturation of the wave amplitude.

Eulerian schemes are compatible with nonuniform phase-space grids, which is a particularly useful feature since the resonance velocity varies significantly along the geomagnetic field line. Finite difference (FD) schemes have the advantage of being easy to implement with the expense of requiring a uniform grid. For this reason, FD schemes have not been a method of choice for solving the Vlasov equation in an inhomogenous magnetic field. In this study, using a procedure similar to *Nunn* [1990, 1993], we present the transformation of the Vlasov equation into a resonance-subtracted coordinate system (including relativistic corrections) such that a uniform grid can be used in the new coordinate space. We leverage the coordinate transformation to complete the first successful numerical simulations of nonlinear amplitude growth of the coherent wave instability using a standard upwind FD scheme.

2. Resonant Coordinate Transformation

The full six dimensional $(\vec{r}, \vec{v})$ Vlasov equation is computationally intensive; thus, several authors have used the reduced four dimensional Vlasov equation $(z, \vec{v})$ with the background inhomogeneity incorporated as a gradient term in the equations of motion [*Inan et al.*, 1978]. Additionally, we make the assumption of parallel propagating waves which is a good approximation for ducted VLF signals [*Haque et al.*, 2011]. For an injected VLF signal propagating in one direction along the field line, significant energy exchange occurs

when particles at the local gyroresonance velocity $v_{res} = \left(\frac{\omega_c}{\gamma} - \omega\right)/k$ interact with the wave. Here ω_c is the electron gyrofrequency, γ is the lorentz factor, ω is the wave frequency, and k is the wave number.

The problem in using a uniform phase-space grid in parallel velocity is that the local resonance velocity changes significantly along the magnetic field line forcing coverage of a large range of parallel velocities. However, the scale at which resonant particles change in $v_\parallel$ is on the order of the trapping velocity, $v_{tr} = \left(\frac{4qB_w v_\perp}{mk}\right)^{\frac{1}{2}}$, which is effectively the size of the trap in $v_\parallel$ space. Therefore, to resolve the fine-scale features, $\Delta v_\parallel \sim v_{tr}/10$ at the very least, where $\Delta v_\parallel$ is the grid spacing in the $v_\parallel$ coordinate. For a numerical interaction region of $\pm$5000 km at $L = 4$ and conservative background parameters, a uniform grid can require hundreds to thousands of points in parallel velocity with a large fraction of the grid not contributing to the simulated physics at any given point in space and time. However, if the initial wave frequency of the injected signal is known, the resonance velocity (or equivalently resonant momentum) is a known function of z and $p_\perp$. The following simple coordinate transformation $\hat{p} = p_\parallel - p_{res}(z, p_\perp)$ forces the local resonance condition to occur at $\hat{p} = 0$ where p_{res} is the resonant momentum ($p_{res} = \gamma m v_{res}$). Here $\gamma = \left(1 + \frac{p_\perp^2 + p_\parallel^2}{(mc)^2}\right)$ is evaluated at $p_\parallel = p_{res}$ to give a quadratic equation $Ap_{res}^2 + Bp_{res} + C = 0$. The coefficients A, B, and C are given in equations (1)–(3):

$$A = \left(\frac{k}{m\omega}\right)^2 - \left(\frac{1}{mc}\right)^2 \tag{1}$$

$$B = -\frac{2k\omega_c}{m\omega^2} \tag{2}$$

$$C = \left(\frac{\omega_c}{\omega}\right)^2 - \left(\frac{p_\perp}{mc}\right)^2 - 1 \tag{3}$$

The root that gives the nonrelativistic resonance velocity in the limit $\gamma \sim 1$ is selected for the coordinate transformation. In canonical coordinates the Vlasov equation is given by equation (4).

$$\frac{\partial f}{\partial t} + \sum_{i=1}^{n} \frac{\mathrm{d}x_i}{\mathrm{d}t} \frac{\partial f}{\partial x_i} = 0 \tag{4}$$

The terms $\frac{\mathrm{d}x_i}{\mathrm{d}t}$ are governed by the single-particle equations of motion (Lorentz force). The Vlasov equation can be readily transformed from one coordinate system to another ($x_i \rightarrow y_j$) using $\frac{\mathrm{d}y_j}{\mathrm{d}t} = \sum_{i=1}^{n} \frac{\partial y_j}{\partial x_i} \frac{dx_i}{\mathrm{d}t}$ and substituting ($x_i \rightarrow y_j$) in equation (4). A significant amount of previous research has used a cylindrical coordinate system ($v_\parallel, v_\perp, \phi, z$) for the equations of motion [*Inan et al.*, 1978; *Dysthe*, 1971]. The new coordinates simply replace $p_\parallel$ with $\hat{p}$ to give ($\hat{p}, p_\perp, \phi, z$). Since p_{res} is only a function of z and $p_\perp$, the equation of motion becomes $\frac{\mathrm{d}\hat{p}}{\mathrm{d}t} = \frac{\mathrm{d}p_\parallel}{\mathrm{d}t} - \frac{\mathrm{d}p_\perp}{\mathrm{d}t}\frac{\partial p_{res}}{\partial p_\perp} - v_\parallel \frac{\partial p_{res}}{\partial z}$. The terms $\frac{\partial p_{res}}{\partial p_\perp}$ and $\frac{\partial p_{res}}{\partial z}$ can be evaluated analytically or numerically. The Vlasov equation in the new coordinate system is then given by equation (5).

$$\frac{\partial f}{\partial t} + \left(\frac{\mathrm{d}z}{dt}\right)\frac{\partial f}{\partial z} + \left(\frac{\mathrm{d}p_\perp}{\mathrm{d}t}\right)\frac{\partial f}{\partial p_\perp} + \left(\frac{\mathrm{d}\phi}{\mathrm{d}t}\right)\frac{\partial f}{\partial \phi} + \left(\frac{\mathrm{d}\hat{p}}{\mathrm{d}t}\right)\frac{\partial f}{\partial \hat{p}} = 0 \tag{5}$$

3. Numerical Model

In the new coordinate system, we employ a first-order accurate linear upwind difference scheme which is diffusive but still provides a physically reasonable solution for a monochromatic input. The scheme works by appropriately discretizing the derivatives using forward or backward finite differencing depending on the direction in phase space that particles stream from. Equation (6) shows the upwind scheme explicitly.

$$f(t + \Delta t) = f(t) - \Delta t \left(\sum_{i=1}^{n} \frac{\mathrm{d}x_i^+}{\mathrm{d}t} D_i^- f + \frac{\mathrm{d}x_i^-}{\mathrm{d}t} D_i^+ f\right) \tag{6}$$

Here $\frac{\mathrm{d}x_i^+}{\mathrm{d}t} = \max\left(\frac{\mathrm{d}x_i}{\mathrm{d}t}, 0\right)$ and $\frac{\mathrm{d}x_i^-}{\mathrm{d}t} = \min\left(\frac{\mathrm{d}x_i}{\mathrm{d}t}, 0\right)$. The quantities $D_i^- f$ and $D_i^+ f$ denote the backward and forward finite difference operators, respectively. The primary bottleneck of explicit finite difference schemes

is that they are constrained by the Courant-Friedrichs-Lewy (CFL) condition, which states that particles can traverse at most one phase-space grid cell in one time step. This enforces that the numerical domain of dependence contains the analytical domain of dependence and is a necessary condition for numerical stability. For the case of the Vlasov equation, the CFL condition is given by $\Delta t < C_{\max}\left(\sum_{i=1}^{n}\frac{\frac{dx_i}{dt}}{\Delta x_i}\right)^{-1}$. Here Δx_i represent the phase-space grid spacings, and $C_{\max}$ is generally a number less than 1. For the investigations described herein, $C_{\max}$ is set to 0.8 which is a conservative value. The time step is then selected using $\Delta t = C_{\max}\left(\sum_{i=1}^{n}\frac{\frac{dx_i}{dt}}{\Delta x_i}\right)^{-1}$. Since this quantity can change with every iteration, the time step is forced to change dynamically.

Since the waves in this simulation are coherent, the Vlasov equation can be coupled to the narrowband wave equations that also take the background cold plasma into account [*Nunn*, 1974]. The narrowband equations are shown in equations (7) and (8).

$$\frac{\partial B_w}{\partial t} - v_g\frac{\partial B_w}{\partial z} = -\frac{\mu_0 v_g}{2}J_E \tag{7}$$

$$\frac{\partial \phi_w}{\partial t} - v_g\frac{\partial \phi_w}{\partial z} = -\frac{\mu_0 v_g}{2}\frac{J_B}{B_w} \tag{8}$$

The quantities B_w and ϕ_w are the wave amplitude and phase of the modulating wave packet propagating in the $-z$ direction at the group velocity, v_g. J_E and J_B are components of the resonant current in the direction of the wave electric and magnetic fields, respectively. Since the single-particle equations of motion require knowing the wave frequency and wave number at each time step, the wave number is updated using $k = k_0 + \frac{\partial \phi_w}{\partial z}$ and the wave frequency can be updated using $\omega = \omega_0 + \frac{\partial \phi_w}{\partial t}$. The time derivative can be removed with the help of equation (8) to give $\omega = \omega_0 - \frac{\mu_0 v_g}{2}\frac{J_B}{B_w} + v_g\frac{\partial \phi_w}{\partial z}$. Here ω_0 and k_0 are the initial wave frequency and wave number and are given by the cold plasma dispersion relation.

The advantage of using the narrowband wave equations is that for a coherent wave, both B_w and ϕ_w will be slowly varying functions of position even if the quantity $B_w e^{i\phi_w}$ may be varying rapidly. Therefore, the number of spatial grid points can be much fewer than if the wave equations were solved in vector form. The disadvantage is that the phase evolution equation (equation (8)) can become unstable for small wave amplitudes due to the B_w term in the denominator. However, for a zero order distribution function that is conducive to growth, the wave amplitude in our simulations was not observed to become small enough to be a concern for the simulations. For simulations with an arbitrary input signal (not monochromatic), solving the vectorized version of the wave equations along with more spatial grid points would be advantageous.

Since the narrowband wave equations are also advective equations (with a source), they can also be solved with the same finite difference scheme used for the Vlasov equation. The wave equations are also constrained by a CFL condition, and the time step that is more restrictive (either for particles or wave) is selected for the simulations. It is also worth noting that no artificial filtering is required for stability of the algorithm.

4. Modeling Results

Since the objective of this study is to model wave amplification of injected coherent signals, we use parameters associated with the Siple Station wave injection experiment [*Helliwell*, 1983]. Particularly, the simulation parameters are $L = 4$, $N_{\text{cold}} = 250$ el/cm^3. The hot plasma distribution function considered is a bi-Maxwellian with $\frac{T_\perp}{T_\parallel} = 2.16$. Additionally, we use $N_{\hat{p}} \times N_{p_\perp} \times N_\phi \times N_z = 101 \times 24 \times 32 \times 400$ for a total of 31 million grid points.

The grid in $\hat{p}$ space ranges ± 5 trapping velocities around $\hat{p} = 0$ where the trapping velocity is evaluated at the average perpendicular momentum and at the maximum wave amplitude predicted by linear theory. This grid is large enough to accommodate approximately a ± 300 Hz change in the wave frequency and still contain the resonance velocity in the simulation space. A full grid is used in $p_\perp$ such that range of pitch angles in the simulations is between 20 and 80°. The input wave amplitude used in the simulation is $B_w = 100fT$ (-20 dB-pT). The initial amplitude filling the simulation space cannot be set to zero due to the B_w term in the denominator of equation (8) and is initialized to 120 dB below the input wave amplitude.

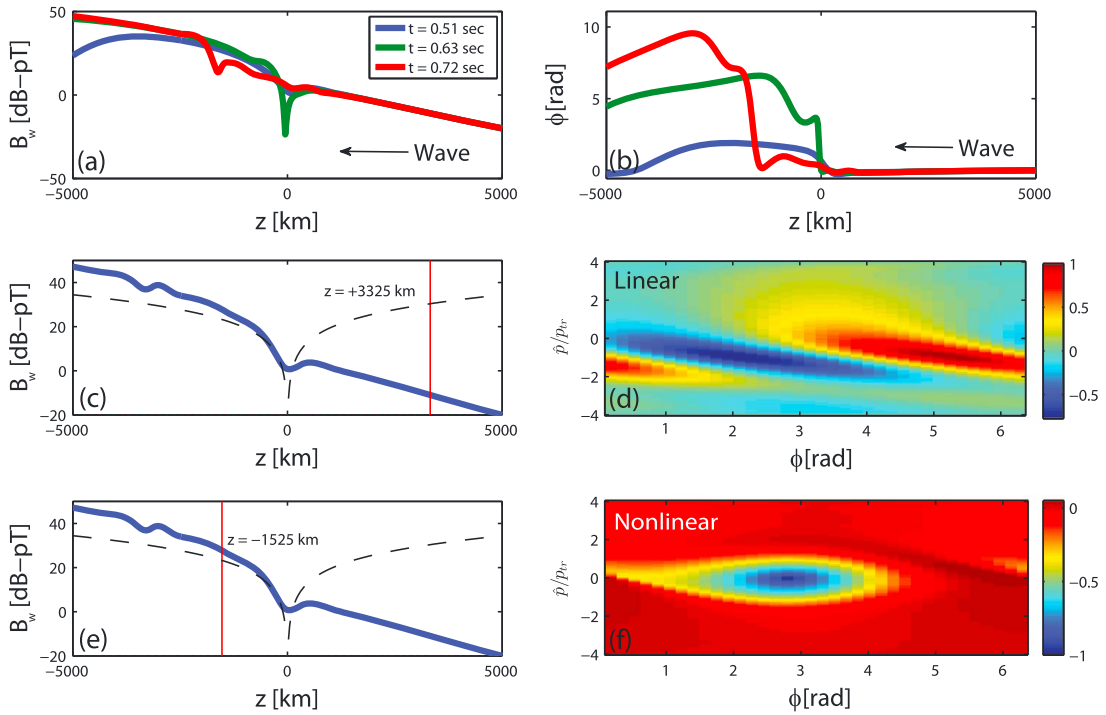

Figure 1. (a and b) The wave amplitude and phase, respectively, at three different time samples ($f_0 = 4.5$ kHz). The wave amplitude grows according to linear theory for $z > 0$ and becomes nonlinear for $z < 0$ after crossing the trapping threshold. As shown in Figure 1b, a nonzero phase shift occurs only for $z < 0$ (nonlinear region) and is responsible for the changing frequency of a triggered emission. (c) The wave amplitude profile once the wave has filled the simulation space ($t = 0.8$ s). (d) The phase-space distribution (integrated over $p_\perp$) in the linear growth regime ($z = 3325$ km). (e and f) The wave profile as well as the phase-space distribution in the nonlinear regime ($z = -1525$ km). In the nonlinear regime, there is a clear depletion in phase space within the trap resulting in a stable "phase-space hole." The dashed black curves in Figures 1c and 1e represent the minimum amplitude required for phase trapping.

Figure 1 shows the results of a simulation with a 4.5 kHz initial frequency and $N_{hot} = 0.5$ el/cm^3. Figures 1a and 1b show the wave amplitude and phase profiles, respectively, at three different snapshots in time. As shown in Figure 1b, the phase profiles only change significantly after sustained crossing of the trapping threshold (shown by the dashed curves), which occurs after the wave has passed the equator, i.e., for $z < 0$. Figures 1c and 1e shows the amplitude profile after the wave has filled the simulation space ($t = 0.8$ s). As shown, the wave amplitude grows according to linear theory before crossing the equator ($z > 0$). The perturbation to the phase-space distribution in $(\hat{p}, \phi)$ space (integrated over $p_\perp$) is shown in Figures 1d and 1f at two positions $z = +3325$ km and $z = -1525$ km, respectively. The distribution functions shown are first subtracted from the unperturbed distribution and then normalized to the maximum value. The distribution in Figure 1d corresponds to the linear regime. Close to the equator, the wave amplitude starts to deviate from the prediction of linear theory. The phase-space distribution well into the nonlinear regime is shown in Figure 1f, and a strong depletion in phase-space density inside the phase trap, resulting in a "phase-space hole" [*Nunn*, 1974; *Omura et al.*, 1991], is clearly visible. The hole is created since particles trapped downstream (of the wave) stay trapped at resonance for several trapping periods and, by Liouville's theorem, will drag the value of the phase-space density from the region downstream where they were first trapped. Since the resonance velocity increases with distance away from the equator, the phase-space density will be lower inside the trap than outside and is thus referred to as a "hole" [*Omura and Nunn*, 2011]. The depth of the hole varies as a function of time and depends on the trapping history of particles and can even be negative (hill instead of a hole) on the upstream side if the wave amplitude is above the trapping threshold. The theoretical idea of the phase-space hole has been proposed by several authors, and our model serves as useful validation of this concept. The well-defined boundaries and shape of the phase-space hole in Figure 1d can be contrasted with the result shown in Figure 7 of *Hikishima and Omura* [2012] that was obtained using a full electromagnetic-PIC simulation. The ability to clearly resolve details in phase space is one of the primary advantages of using an Eulerian Vlasov solver.

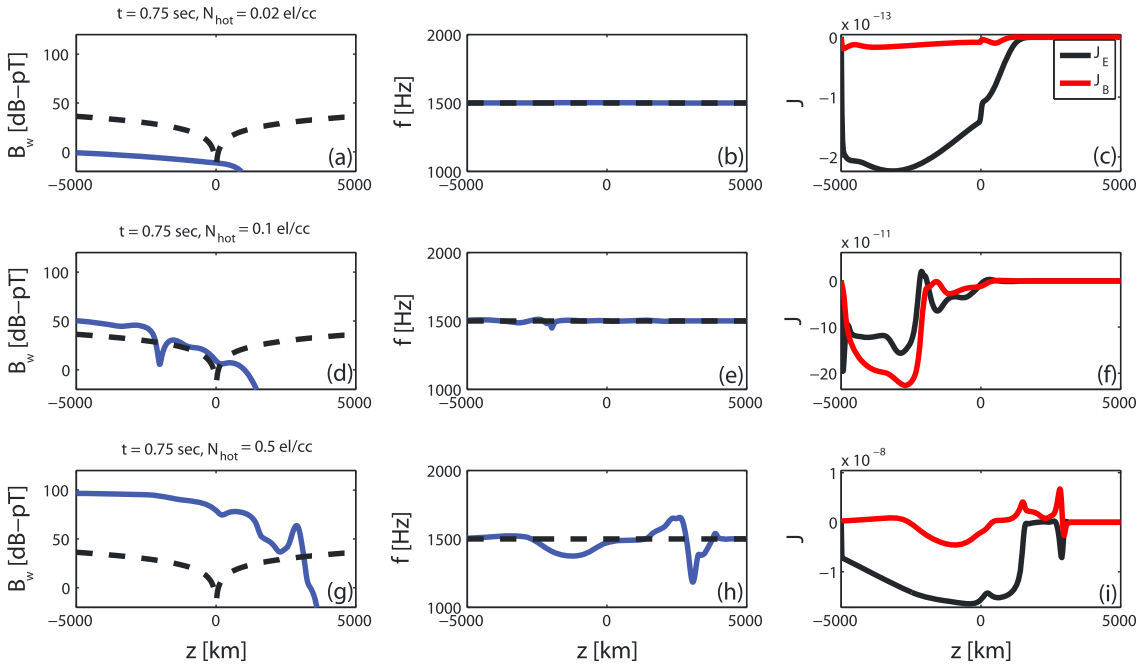

Figure 2. (a–c) The wave amplitude, wave frequency, and currents, respectively, for N_{hot} = 0.02 el/cm^3. The wave growth is purely linear in this case, and there is no frequency change since the amplitude does not cross the trapping threshold. (d–f) The amplitude, frequency, and resonant current profiles for N_{hot} = 0.1 el/cm^3. The wave growth crosses the trapping threshold in this case which occurs primarily for $z < 0$. Although the wave amplitude is large enough to be nonlinear, the frequency change is still small as shown in Figure 2e. (g–i) The amplitude, frequency, and currents for N_{hot} = 0.5 el/cm^3. The linear growth rate is extremely high in this case (625 dB/s) and crosses the trapping threshold much before the wave crosses the equator. The wave growth is subsequently nonlinear with a nonzero frequency change that resembles a triggered emission.

The reason nonlinear growth occurs primarily for ($z < 0$) in the results shown in Figure 1 is that linear growth brings the wave amplitude up to trapping threshold only very close to magnetic equator. If the linear growth rate or the injected wave amplitude were higher, the trapping threshold would be crossed sooner and nonlinear growth would initiate before the wave reaches the equator. To examine the transition from linear to nonlinear growth, we consider three simulations with three different hot plasma densities (N_{hot} =,0.02, 0.1, and 0.5 el/cm^3) at f_0 = 1.5 kHz with an input pulse duration of 0.5 s. The corresponding equatorial linear growth rates are 25, 125, and 625 dB/s. The simulation results are shown in Figure 2, with each row corresponding to one simulation. Figures 2a, 2d, and 2g show the wave amplitude as a function of position, Figures 2b, 2e, and 2h show the wave frequency, and Figures 2c, 2f, and 2i show the corresponding resonant currents (J_E and J_B). Figures 2a–2c show the wave and current profiles at t = 0.75 s for N_{hot} = 0.02 el/cm^3. As shown, this case has the lowest hot plasma density, the wave amplitude does not cross the trapping threshold (shown by the dashed black curve) and the growth is well described by linear theory. In this linear regime, the frequency does not change from the injected value of 1500 Hz. This is because the component of the current in the direction of the wave magnetic field (J_b) is responsible for frequency change and should be identically zero according to linear plasma theory. As shown in Figure 2c, J_B is approximately an order of magnitude less than J_E and linear theory is thus accurate in this case. Figures 2d–2f show the wave and current profiles for N_{hot} = 0.1 el/cm^3. In this case, the linear growth was high enough to make the wave amplitude exceed the trapping threshold. As shown, the amplitude crosses the threshold very close to the equator which is similar to the case in Figure 1. Figure 2e shows the frequency profile which has not deviated much from the original 1500 Hz even where the wave growth is nonlinear. The current profiles in Figure 2f are largest for $z < 0$ where the wave amplitude is above the trapping threshold and hence nonlinear. The last case, with N_{hot} = 0.5 el/cm^3, is shown in Figures 2g–2f. In this case, the wave amplitude crosses the trapping threshold significantly before the wave passes the equator. The wave subsequently undergoes significant nonlinear growth and reaches values of approximately 100 dB-pT at the exit of the simulation space. Note that the back end of the pulse does not look like it has traveled as far as the cases with the lower hot plasma densities (Figures 2a and 2d). This occurs because particles that leave the back

end of the pulse are forced to fall out of the trap and radiate additional wave energy in the process. This extends the pulse length as well as changes the wave frequency which is shown in Figure 2h. The frequency deviation is continuous but not at a constant sweep rate. This is consistent with *Nunn et al.* [2005] where hooks and oscillating tones were found for cases with the largest wave amplitudes. In this simulation, the frequency change (triggering) occurs close to where the wave crosses the trapping threshold and essentially propagates away from that location. This result suggests that the transition from trapping to detrapping of resonant particles plays an important role in the triggering free-running emissions.

Although the model reproduces nonlinear growth and frequency change that can resemble a triggered emission, it is worth noting that the first-order upwind scheme is known to be dissipative when large gradients are formed. Incorporating a higher-order finite difference scheme for the Vlasov-Maxwell solver is a subject of future research.

5. Conclusion

We have shown that coherent wave amplification can be modeled using a finite difference scheme on a uniform grid after transforming to a resonance-subtracted coordinate system. We used a first-order upwind scheme which is the simplest stable scheme but is diffusive. With this scheme, the model demonstrates both linear as well as nonlinear growth, with the formation of a stable and well-defined phase-space hole during the nonlinear growth process. The point at which the transition from linear to nonlinear takes place depends on the linear growth rate such that linear growth can raise the wave amplitude above the trapping threshold. For low growth rates, the amplification is purely linear since the trapping threshold is never exceeded. For the case with a large linear growth rate, the trapping threshold is crossed quickly and a continuous change in frequency takes place close to where the wave first crosses the threshold and propagates away from there. This suggests that particles leaving the back end of the wave trap are an important part of the triggering process.

Acknowledgments

This work has been supported by AFRL award FA9453-11-C-0011 to Stanford University and subcontract 27239350-50917-B to CU Denver. Mark Gołkowski acknowledges additional support from NSF CAREER award AGS 1254365. All data used in this study can be accessed by contacting the authors.

W.K. Peterson thanks David Nunn and one anonymous reviewer for their assistance in evaluating this paper.

References

Abel, B., and R. M. Thorne (1998), Electron scattering loss in Earth's inner magnetosphere: 1. Dominant physical processes, *J. Geophys. Res.*, *103*, 2385–2396, doi:10.1029/97JA02919.

Albert, J. M., X. Tao, and J. Bortnik (2012), Aspects of nonlinear wave-particle interactions, in *Dynamics of the Earth's Radiation Belts and Inner Magnetosphere, Geophys. Monogr. Ser.*, vol. 199, edited by D. Summers et al., pp. 255–264, AGU, Washington, D. C.

Bell, T. F., and O. Buneman (1964), Plasma instability in the whistler mode caused by a gyrating electron stream, *Phys. Rev.*, *133*, 1300–1302, doi:10.1103/PhysRev.133.A1300.

Bortnik, J., and R. Thorne (2007), The dual role of ELF/VLF chorus waves in the acceleration and precipitation of radiation belt electrons, *J. Atmos. Sol. Terr. Phys.*, *69*(3), 378–386.

Dysthe, K. B. (1971), Some studies of triggered whistler emissions, *J. Geophys. Res.*, *76*(28), 6915–6931, doi:10.1029/JA076i028p06915.

Filbet, F., and E. Sonnendrücker (2003), Comparison of Eulerian Vlasov solvers, *Comput. Phys. Commun.*, *150*(3), 247–266, doi:10.1016/S0010-4655(02)00694-X.

Gibby, A. R., U. S. Inan, and T. F. Bell (2008), Saturation effects in the VLF-triggered emission process, *J. Geophys. Res.*, *113*, A11215, doi:10.1029/2008JA013233.

Haque, N., U. S. Inan, T. F. Bell, J. S. Pickett, J. G. Trotignon, and G. Facskó (2011), Cluster observations of whistler mode ducts and banded chorus, *Geophys. Res. Lett.*, *38*, L18107, doi:10.1029/2011GL049112.

Harid, V., M. Gołkowski, T. Bell, and U. S. Inan (2014), Theoretical and numerical analysis of radiation belt electron precipitation by coherent whistler mode waves, *J. Geophys. Res. Space Physics*, *119*, 4370–4388, doi:10.1002/2014JA019809.

Helliwell, R. A. (1983), Controlled stimulation of VLF emissions from Siple Station, Antarctica, *Radio Sci.*, *18*(6), 801–814.

Hikishima, M., and Y. Omura (2012), Particle simulations of whistler-mode rising-tone emissions triggered by waves with different amplitudes, *J. Geophys. Res.*, *117*, A04226, doi:10.1029/2011JA017428.

Hikishima, M., S. Yagitani, Y. Omura, and I. Nagano (2009), Full particle simulation of whistler-mode rising chorus emissions in the magnetosphere, *J. Geophys. Res.*, *114*, A01203, doi:10.1029/2008JA013625.

Hikishima, M., Y. Omura, and D. Summers (2010), Self-consistent particle simulation of whistler mode triggered emissions, *J. Geophys. Res.*, *115*, A12246, doi:10.1029/2010JA015860.

Inan, U. S., T. F. Bell, and R. A. Helliwell (1978), Nonlinear pitch angle scattering of energetic electrons by coherent VLF waves in the magnetosphere, *J. Geophys. Res.*, *83*(A7), 3235–3253, doi:10.1029/JA083iA07p03235.

Katoh, Y., and Y. Omura (2006), A study of generation mechanism of VLF triggered emission by self-consistent particle code, *J. Geophys. Res.*, *111*, A12207, doi:10.1029/2006JA011704.

Katoh, Y., and Y. Omura (2007), Computer simulation of chorus wave generation in the Earth's inner magnetosphere, *Geophys. Res. Lett.*, *34*, L03102, doi:10.1029/2006GL028594.

Kennel, C. F., and H. E. Petschek (1966), Limit on stably trapped particle fluxes, *J. Geophys. Res.*, *71*, 1–28.

Nunn, D. (1974), A self-consistent theory of triggered VLF emissions, *Planet. Space Sci.*, *22*, 349–378, doi:10.1016/0032-0633(74)90070-1.

Nunn, D. (1990), The numerical simulation of VLF nonlinear wave-particle interactions in collision-free plasmas using the Vlasov hybrid simulation technique, *Comput. Phys. Commun.*, *60*(1), 1–25, doi:10.1016/0010-4655(90)90074-B.

Nunn, D. (1993), A novel technique for the numerical simulation of hot collision-free plasma; Vlasov hybrid simulation, *J. Comput. Phys.*, *108*(1), 180–196, doi:10.1006/jcph.1993.1173.

Nunn, D., and Y. Omura (2012), A computational and theoretical analysis of falling frequency VLF emissions, *J. Geophys. Res.*, *117*, A08228, doi:10.1029/2012JA017557.

Nunn, D., and A. J. Smith (1996), Numerical simulation of whistler-triggered VLF emissions observed in Antarctica, *J. Geophys. Res.*, *101*(A3), 5261–5277, doi:10.1029/95JA03143.

Nunn, D., Y. Omura, H. Matsumoto, I. Nagano, and S. Yagitani (1997), The numerical simulation of VLF chorus and discrete emissions observed on the geotail satellite using a Vlasov code, *J. Geophys. Res.*, *102*(A12), 27,083–27,097, doi:10.1029/97JA02518.

Nunn, D., A. Demekhov, V. Trakhtengerts, and M. Rycroft (2003), Vlf emission triggering by a highly anisotropic energetic electron plasma, *Ann. Geophys.*, *21*, 481–492.

Nunn, D., M. Rycroft, and V. Trakhtengerts (2005), A parametric study of the numerical simulations of triggered VLF emissions, *Ann. Geophys.*, *23*, 3655–3666.

Omura, Y., and D. Nunn (2011), Triggering process of whistler mode chorus emissions in the magnetosphere, *J. Geophys. Res.*, *116*, A05205, doi:10.1029/2010JA016280.

Omura, Y., H. Matsumoto, D. Nunn, and M. J. Rycroft (1991), A review of observational, theoretical and numerical studies of VLF triggered emissions, *J. Atmos. Terr. Phys.*, *53*, 351–368.

Omura, Y., Y. Katoh, and D. Summers (2008), Theory and simulation of the generation of whistler-mode chorus, *J. Geophys. Res.*, *113*, A04223, doi:10.1029/2007JA012622.

Thorne, R., et al. (2013), Rapid local acceleration of relativistic radiation-belt electrons by magnetospheric chorus, *Nature*, *504*(7480), 411–414.

Thorne, R. M. (2010), Radiation belt dynamics: The importance of wave-particle interactions, *Geophys. Res. Lett.*, *37*, L22107, doi:10.1029/2010GL044990.

Thorne, R. M., B. Ni, X. Tao, R. B. Horne, and N. P. Meredith (2010), Scattering by chorus waves as the dominant cause of diffuse auroral precipitation, *Nature*, *467*(7318), 943–946.